

Lithium Abundances of Extremely Metal-Poor Turn-off Stars¹

Wako Aoki^{2,3}, Paul S. Barklem⁴, Timothy C. Beers⁵, Norbert Christlieb⁶, Susumu Inoue^{2,7}, Ana E. García Pérez⁸, John E. Norris⁹, Daniela Carollo^{9,10}

ABSTRACT

We have determined Li abundances for eleven metal-poor turn-off stars, among which eight have $[\text{Fe}/\text{H}] < -3$, based on LTE analyses of high-resolution spectra obtained with the HDS on the Subaru telescope. The Li abundances for four of these eight stars are determined for the first time by this study. Effective temperatures are determined by a profile analysis of $\text{H}\alpha$ and $\text{H}\beta$. While seven stars have Li abundances as high as the Spite Plateau value, the remaining four objects with $[\text{Fe}/\text{H}] < -3$ have $A(\text{Li}) = \log(\text{Li}/\text{H}) + 12 \lesssim 2.0$, confirming the existence of extremely metal-poor turn-off stars having low Li abundances, as reported by previous work. The average of the Li abundances for stars with $[\text{Fe}/\text{H}] < -3$ is lower by 0.2 dex than that of the stars with higher metallicity. No clear constraint on the metallicity dependence or scatter of the Li abundances is derived from our measurements for the stars with $[\text{Fe}/\text{H}] < -3$. Correlations of the Li abundance with effective temperatures, with abundances of Na, Mg and Sr, and with the kinematical properties are investigated, but no clear correlation is seen in the extremely metal-poor star sample.

Subject headings: nuclear reactions, nucleosynthesis, abundances – stars: abundances – stars: Population II

²National Astronomical Observatory, Mitaka, Tokyo, 181-8588 Japan; email: aoki.wako@nao.ac.jp

³Department of Astronomical Science, The Graduate University of Advanced Studies, Mitaka, Tokyo, 181-8588 Japan

⁴Department of Physics and Astronomy, Uppsala University, Box 515, 751-20 Uppsala, Sweden; email: Paul.Barklem@physics.uu.se

⁵Department of Physics and Astronomy, CSCE: Center for the Study of Cosmic Evolution, and JINA: Joint Institute for Nuclear Astrophysics, Michigan State University, East Lansing, MI 48824-1116; email: beers@pa.msu.edu

⁶University of Heidelberg, ZAH, Landessternwarte Königstuhl 12, D-69117 Heidelberg, Germany, N.Christlieb@lsw.uni-heidelberg.de

⁷Present address: Department of Physics, Kyoto University, Oiwake-cho, Kitashirakawa, Sakyo-ku, Kyoto 606-8502, Japan; email: inoue@tap.scphys.kyoto-u.ac.jp

⁸Centre for Astrophysics Research, STRI and School of Physics, Astronomy and Mathematics, University of Hertfordshire, College Lane, Hatfield AL10 9AB, United Kingdom; email: a.e.garcia-perez@herts.ac.uk

⁹Research School of Astronomy and Astrophysics, The Australian National University, Mount Stromlo Observatory, Cotter Road, Weston, ACT 2611, Australia; email: jen@mso.anu.edu.au, carollo@mso.anu.edu.au

¹⁰INAF-Osservatorio Astronomico di Torino, Italy

1. Introduction

Over the course of the past few decades, Li abundances have been measured for many metal-poor main-sequence turn-off stars, in hopes of placing constraints on the nature of Big Bang nucleosynthesis (BBN). The first such investigation, by Spite & Spite (1982), revealed that warm metal-poor main-sequence stars exhibited a constant Li abundance. This so-called Spite Plateau was interpreted as a result of the synthesis of light nuclei in the first several minutes of the evolution of the Universe (it is conventionally assumed that Li is not destroyed at the surface of such stars because of their shallow surface convection zones). Since then, measurements of Li abundances have been obtained over wide ranges of effective temperature and metallicity, confirming that the scatter of the Li abundances in most stars with $T_{\text{eff}} > 5700$ K and $[\text{Fe}/\text{H}] < -1.5$ is small, if present at all (Ryan et al. 1999, and references therein)².

However, it has been recognized that the Spite Plateau value of $A(\text{Li})$ (~ 2.2) is 0.3–0.4 dex lower than the Li abundance predicted by standard BBN models (Coc et al. 2004), adopting the baryon density determined by recent measurements of the cosmic microwave background (CMB) radiation with the WMAP satellite (Spergel et al. 2003). This discrepancy indicates the existence of poorly understood processes that deplete Li in metal-poor turn-off stars (e.g. Korn et al. 2006, 2007), astration of Li in the gas that formed these stars (perhaps by massive zero-metallicity progenitors; Piau et al. 2006), problems in the measured abundances of Li in metal-poor stars, systematic uncertainties in the standard BBN model predictions, or exotic processes in the early universe arising from nonstandard particle physics (Cyburt et al. 2008 and references therein).

Recent measurements of very metal-poor turn-off stars also suggest a decreasing trend of Li abundances with decreasing metallicity (Ryan et al. 1996, 1999; Boesgaard et al. 2005; Asplund et al. 2006). In particular, Bonifacio et al. (2007) investigated the Li abundances for a sample that includes eight stars with $[\text{Fe}/\text{H}] < -3$. They showed that the Li abundances of these stars are lower than those of stars with higher metallicity, investigating very carefully the scatter and trend of Li abundances with metallicity and effective temperature.

Another unsolved problem is the low Li abundance found in HE 1327–2326, a hyper metal-poor turn-off star having $[\text{Fe}/\text{H}] < -5$ (Frebel et al. 2005; Aoki et al. 2006). Only an upper-limit on the Li abundance has been determined, $A(\text{Li}) < +0.62$ (Frebel et al. 2008). Although the star has probably evolved to the subgiant branch (Korn et al. 2009), the effective temperature of this object (6180 K; Frebel et al. 2005) is still sufficiently high that depletion of Li by surface convection is not expected. Another possible explanation for the apparent depletion of Li is mass accretion from an evolved companion star (Ryan et al. 2002), in particular because this star is highly carbon-

¹Based on data collected at the Subaru Telescope, which is operated by the National Astronomical Observatory of Japan.

² $[A/B] = \log(N_A/N_B) - \log(N_A/N_B)_\odot$, and $\log \epsilon_A = \log(N_A/N_H) + 12$ for elements A and B. Lithium abundances are conventionally presented as $A(\text{Li})$ instead of $\log \epsilon_{\text{Li}}$.

enhanced ($[\text{C}/\text{Fe}] \sim +4.0$; Aoki et al. 2006). However, no signature of binarity has been found yet for this object (Frebel et al. 2008).

Thus, concerning the ${}^7\text{Li}$ abundances in very metal-poor stars, we are confronted with three problems: (1) The discrepancy between the observed Spite Plateau value and the prediction of standard BBN models adopting the baryon density determined by CMB measurements; (2) A possible trend of the Li abundance as a function of metallicity in extremely metal-poor stars; and (3) The low Li abundance in HE 1327–2326 (see also the summary by Piau et al. 2006). Although possible connections between the above three problems are still unknown, we have obtained measurements of Li abundances for several extremely metal-poor turn-off stars in a search for hints to solving these Li puzzles.

In this paper we report measurements of Li abundances for very and extremely metal-poor stars. Our sample includes eight stars with $[\text{Fe}/\text{H}] < -3$, among which four stars are studied for the first time. The sample selection and high-resolution spectroscopy are described in § 2. Section 3 reports the determination of stellar parameters and details of the measurement of Li abundances. Uncertainties and comparisons with previous work are also discussed in this section. We discuss the implications of our measurements in § 4, and consider possible correlations with the derived stellar atmospheric parameters, other elemental abundances, and the kinematics of the sample.

2. Observations

High-resolution spectra of very and extremely metal-poor main-sequence turn-off stars were obtained in the course of three different observing programs, using the Subaru Telescope High Dispersion Spectrograph (HDS; Noguchi et al. 2002). Table 1 lists the objects and details of the observations. The spectra of the first five objects were obtained in an observing program for extremely metal-poor stars in 2005 (Aoki et al. 2006). The two objects from the SDSS sample were observed in a program for Carbon-Enhanced Metal-Poor (CEMP) stars (Aoki et al. 2008). Although these two stars were selected as candidate CEMP turn-off stars having $[\text{Fe}/\text{H}] < -3$, they turned out to show no clear carbon excess in our high-resolution spectroscopy, thus were good targets for studying the Li abundances in the extremely low metallicity range. The other four bright stars were observed with very high signal-to-noise (S/N) ratios in order to measure Li isotope ratios (P.I. S. Inoue).

Lithium abundances for seven objects in our sample have been recently measured with high-resolution spectroscopy by other authors. The stars CS 22948–093 and CS 22965–054 were studied by Bonifacio et al. (2007). The five bright objects are well-known stars for Li studies. BD+26°3578 was recently studied by Asplund et al. (2006). Li abundances of G 64–12 and G 64–37 were measured by Ryan et al. (1999) and Boesgaard et al. (2005). Ryan et al. (1999) also determined Li abundances for HD 84937, BD+26°3578 and CD –24°17504. Duplications of targets with previous studies provide the opportunity to examine the consistency between independent abundance mea-

surements. The Li abundances of the other four stars (BS 16545–089, HE 1148–0037, SDSS 0040+16 and SDSS 1033+40) are reported for the first time by the present study.

The spectral resolution for the last four stars in Table 1 is $R = 90,000$ or $100,000$. The other objects were observed with $R = 60,000$ with 2×2 CCD on-chip binning. An exception is SDSS 1033+40, which was observed with $R = 45,000$ to collect sufficient photons, using a wider slit, under relatively poor seeing conditions. The spectra cover 4100–6800 Å, although the coverage is slightly different between the individual observing programs.

Data reduction was carried out with standard procedures using IRAF³. Photon counts at 6700 Å are listed in Table 1. Spectra of this wavelength region are shown in Figure 1. Equivalent widths of Fe, Na, Mg, and Sr lines were measured by fitting Gaussian profiles, in order to determine atmospheric parameters and chemical compositions. Since the Li I $\lambda 6708$ line consists of a doublet, Gaussian fitting is not appropriate for the measurement of equivalent widths. Instead, we determined the Li abundances by fitting synthetic spectra (§3.3). For comparisons of equivalent widths with previous studies, we measured the equivalent widths of this line from the synthetic spectra (§3) that provided the best fits to the observed ones. The equivalent widths of the interstellar Na I D lines, which can be used to estimate the interstellar reddening (§3), were measured by direct integration of the absorption features.

The heliocentric radial velocities listed in Table 1 were measured from the same clean Fe I lines that were used to determine iron abundances. The uncertainty given in Table 1 is σ_v/N , where σ_v is the standard deviation of the measurements and N is the number of lines used. In addition, one should take into account possible small systematic errors due to the instability of the instrument, which are at most 0.4 km s^{-1} (Aoki et al. 2005).

3. Stellar Parameters and Li Abundance Measurements

3.1. Effective Temperatures

The effective temperatures (T_{eff} 's) of our program stars were determined from profile fits to hydrogen Balmer lines, a technique used as well by Asplund et al. (2006) and Bonifacio et al. (2007). We employed the H α and H β lines [$T_{\text{eff}}(\text{H}\alpha)$ and $T_{\text{eff}}(\text{H}\beta)$]. Although H γ is also covered by our observations, it lies at the edge of the CCD, making continuum rectification difficult, and thus has not been used. The method for continuum rectification of the observed spectra and analysis used follows exactly that described in Barklem et al. (2002), which may be consulted for details. The most important aspects of the analysis are that the synthetic profiles are computed assuming LTE line formation using 1D LTE plane-parallel MARCS models (Asplund et al. 1997), with convection

³IRAF is distributed by the National Optical Astronomy Observatories, which is operated by the Association of Universities for Research in Astronomy, Inc. under cooperative agreement with the National Science Foundation.

described by mixing length theory with parameters $\alpha = 0.5$ and $y = 0.5$. The most important line-broadening mechanisms for the wings are Stark broadening and self broadening, which are described by calculations of Stehlé & Hutcheon (1999) and Barklem, Piskunov & O’Mara (2000), respectively. The fitting is accomplished by minimisation of the χ^2 statistic, comparing the observed and synthetic profiles. Essentially the same method was used by Asplund et al. (2006), although with some differences in the rectification and profile comparison techniques.

We note that the assumption of LTE for formation of the Balmer line wings in cool stars has recently been shown to be questionable on the basis of theoretical non-LTE calculations (Barklem 2007), the role of hydrogen collisions being a major uncertainty. Those calculations admit that the temperatures from LTE Balmer line wings could be systematically too cool by of order 100 K if hydrogen collisions are inefficient, although LTE is not ruled out. Due to the fact that there is no strong evidence favoring any particular hydrogen collision model, we chose to calculate in LTE as this temperature scale is well studied, and it is computationally most practical. However, we emphasize that LTE is not a safe middle ground, and will lead to temperatures systematically too cool should departures from LTE exist in reality.

Often, $H\alpha$ is given higher weight than higher series lines such as $H\beta$ for reasons discussed by Fuhrmann et al. (1993). However, in extremely metal-poor turn-off stars this is no longer obvious since blending by metal lines becomes unimportant, and $H\beta$ becomes in fact almost insensitive to gravity, while $H\alpha$ is quite gravity sensitive (see table 4 of Barklem et al. (2002)). Further, the calculations by Barklem (2007) suggest that non-LTE effects, if they exist, will be largest in $H\alpha$. Thus, in combining the temperatures from $H\alpha$ and $H\beta$, we have in fact given $H\beta$ double the weight of $H\alpha$.

The derived effective temperatures are dependent on the gravity assumed in the calculation. The analysis is iterated for the gravity, which is determined from the analysis of the high-resolution spectrum (§ 3) for each object. The results and uncertainties of the T_{eff} determinations are listed in Table 2. The uncertainties listed in the tables are estimated from the quality of the spectrum and the fit.

For comparison purposes, we also estimated the effective temperatures from the $(V - K)_0$ colors $[T_{\text{eff}}(V - K)]$, using the effective temperature scales of Alonso, Arribas, & Martínez-Roger (1996), Ramírez & Meléndez (2005b), and González Hernández & Bonifacio (2009). For the estimates using the scale of Alonso, Arribas, & Martínez-Roger (1996), we assume $[\text{Fe}/\text{H}] = -3.0$ for stars having $[\text{Fe}/\text{H}] < -3.0$ following Ryan et al. (1999). The photometry data were collected from Beers et al. (2007), the 2MASS catalogue (Skrutskie et al. 2006), and the SIMBAD database. The V magnitudes of the SDSS stars are derived from the g magnitude and $g - r$ color, as in Aoki et al. (2008). Interstellar reddening is estimated from the dust maps of Schlegel et al. (1998) and from the interstellar Na I D line, using the scale of Munari & Zwitter (1997); results are listed in Table 3. We adopt the reddening estimate obtained from the Na D line for the brightest four stars (HD 84937, BD+26°3578, G 64–12 and G 64–37) because these are nearby stars, and the reddening might be

overestimated from the dust maps. The interstellar Na D lines blend with the stellar lines in the spectrum of HE 1148–0037, so the reddening value from the dust map is adopted for this object. For the other six objects, the averages of the reddening values derived from the two methods are adopted. The differences between the $E(B - V)$ values based on the two methods are generally 0.01 mag or smaller. The exception is for CS 22965–054, which exhibits the largest $E(B - V)$ among the sample, $E(B - V) = 0.09$ from the dust map and 0.13 from the Na D line. The extinction in each band is obtained from the reddening relation given by Schlegel et al. (1998).

The photometry data and the derived effective temperatures are listed in Table 3. Figure 2 shows the differences between the effective temperatures from Balmer lines and those from $V - K$ colors for the three temperature scales. The effective temperatures from the scales of Ramírez & Meléndez (2005b) and González Hernández & Bonifacio (2009) are systematically higher than those from Alonso, Arribas, & Martínez-Roger (1996). The differences between the results from González Hernández & Bonifacio (2009) and from Alonso, Arribas, & Martínez-Roger (1996) are 100-150 K. The results from Ramírez & Meléndez (2005b) are 100-200 K higher still than those from González Hernández & Bonifacio (2009) for stars with $[\text{Fe}/\text{H}] < -3$, while the agreement is fairly good for the three stars having higher metallicity (shown by smaller symbols in the figure). These differences between the effective temperature scales were already reported by Ramírez & Meléndez (2005b) and González Hernández & Bonifacio (2009).

The comparisons with the results from Balmer line analyses indicate that the effective temperatures from the scale of Alonso, Arribas, & Martínez-Roger (1996) agree in general with those from the Balmer lines. The star showing the largest discrepancy is SDSS 0040+16. This star has a $(V - K)_0$ smaller than the color range ($1.1 < (V - K)_0 < 1.6$) for which the formulae of Alonso et al. are applicable. The results from the scales of González Hernández & Bonifacio (2009) and Ramírez & Meléndez (2005b) for stars with $[\text{Fe}/\text{H}] < -3$ are systematically higher than those from Balmer lines by 150 K and 250 K, respectively.

Determination of the Li abundance is sensitive to the effective temperatures adopted in the analysis. We discuss the impact of effective temperatures on the metallicity dependence of Li abundances in § 4.

The estimate of effective temperatures for extremely metal-poor stars from these temperature scales would be rather uncertain, because of the small number of stars in the sample used to produce the scales. Alonso, Arribas, & Martínez-Roger (1996) includes a very small number of stars for the ranges of the color and metallicity. Ramírez & Meléndez (2005a) increased the number of such stars, which are used to produce the scale of Ramírez & Meléndez (2005b). However, the sample is still not large (10 stars) and includes one carbon-enhanced star and two known double-lined spectroscopic binaries. Further measurements of effective temperatures by the infrared flux method are desired for this metallicity range.

3.2. Other Parameters and Abundances

The abundance analyses were made using the grid of ATLAS9 NEWODF model atmospheres (Kurucz 1993; Castelli & Kurucz 2003), with enhancement of the α -elements. Calculations of synthetic spectra for abundance analyses were made employing a 1D-LTE spectral synthesis code that is based on the same assumptions as the model atmosphere program of Tsuji (1978). The surface gravities ($\log g$) are estimated from the effective temperatures and Y^2 isochrones (Kim et al. 2002) for $[\text{Fe}/\text{H}] = -2.5$ (for HD 84937 and BD+26°3578) and $[\text{Fe}/\text{H}] = -3.5$ (for the others) assuming the ages of these stars to be 12 Gyr. For the T_{eff} range of our sample, two possibilities of $\log g$ exist: the subgiant case ($\log g \sim 3.8$) and the main-sequence case ($\log g \sim 4.4$). We performed abundance analyses for Fe I and Fe II (see below for details), and selected the $\log g$ that provides better agreement of iron abundances from the two species for each star. The derived $\log g$ value is not sensitive to the assumption of the age for selecting isochrones. The results for $\log g$ and the derived iron abundances from the two species are listed in Table 2. We re-determined effective temperature when the gravity assumed in the first estimate of effective temperature is different from the derived one. We note that the Fe abundance from Fe I lines and the Li abundance are not sensitive to the gravity adopted in the analysis.

The analysis, when adopting the micro-turbulent velocity (v_{micro}) of 1.5 km s^{-1} , results in no statistically significant dependence of the iron abundances on the strengths of the Fe I lines used for the analysis for BS 16545–089, HE 1148–0037, G 64–12, G 64–37 and BD+26°3578, while 1.2 km s^{-1} is preferable for HD 84937. Since the number of iron lines available in the abundance analyses of the other four stars is too small to estimate their micro-turbulent velocity, we assume v_{micro} of 1.5 km s^{-1} for these objects. We note that the Li abundance derived from the weak Li I $\lambda 6708$ line is insensitive to the micro-turbulent velocity adopted in the analysis.

In the following discussion, we adopt the iron abundances from Fe I lines (Table 2) as the metallicity. Although the iron abundances from Fe I lines are considered to be possibly affected by non-LTE effects (Asplund 2005, and references therein), our results are insensitive to the gravity adopted in the analysis. We refer to a solar Fe abundance of $\log \epsilon_{\odot}(\text{Fe}) = 7.45$ (Asplund et al. 2005) to derive the $[\text{Fe}/\text{H}]$ and $[\text{X}/\text{Fe}]$ values.

In order to investigate correlations between the abundances of Li and other elements, Na, Mg, and Sr abundances are determined by a standard LTE analysis from the Na I 5890 and 5896 Å lines (D lines), Mg I 5172, 5183, and/or 5528 Å lines, and Sr II 4078 and/or 4215 Å lines, respectively. The agreement of the abundances from two or three lines for each element is fairly good. The results are listed in Table 4. Correlations between the abundances of Li and these elements are examined in § 4. The Na D lines are known to suffer a significant NLTE effect that is dependent on the line strengths. The effect is, however, not large ($\Delta[\text{Na}/\text{Fe}]_{\text{NLTE}} - [\text{Na}/\text{Fe}]_{\text{LTE}} \lesssim 0.1$ dex) for the extremely metal-poor stars that have equivalent widths of the D lines less than $50 \text{ m}\text{\AA}$ (Takeda et al. 2003; Andrievsky et al. 2007). The effect could be larger (~ -0.3 dex) for the less metal-poor stars whose equivalent widths are as large as $100 \text{ m}\text{\AA}$.

3.3. Analyses of the Li Line

The Li abundances are derived from the Li I 6708 Å line by fitting the observed spectra with synthetic spectra. Doppler corrections for the observed spectra are determined by the Fe I line positions used for the above abundance measurements. In the fitting procedure for the four bright stars (HD 84937, BD+26°3578, G 64–12 and G 64–37), a small wavelength shift is included as a fitting parameter (see below). The continuum level is estimated from the wavelength range around the Li line (6706.9–6707.4 Å and 6708.2–6708.7 Å). The list of the Li lines provided by Smith et al. (1998) is adopted, neglecting the contribution of ⁶Li. We assume a Gaussian profile to account for the broadening by macro-turbulence, including rotation, and by the instrument. We assume a broadening of 7 km s⁻¹ for the stars observed with $R \geq 90,000$, and 8 km s⁻¹ for the others, values that sufficiently explain the widths of weak Fe lines. We performed the analyses changing the value by ± 1 km s⁻¹, and confirmed that the effect of the assumed line broadening on the derived ⁷Li abundance is small (~ 0.01 dex).

We then search for the Li abundance that yields the minimum χ^2 . We found that the fit is slightly improved by allowing a small wavelength shift for the four brightest stars, while the effect is negligible for the others. Hence, in our procedure for fitting of the synthetic spectra to the observations, the free parameter was the Li abundance, and for the four brightest stars also a wavelength shift. The number of data points to which the fitting is applied is 18 and 36 for the cases of two pixel binning and of no binning, respectively. The 2σ range is adopted as the fitting error ($\sigma[A(\text{Li})]_{\text{fit}}$ in Table 4). While the fitting errors for the four bright stars (G 64–12, G 64–37, HD 84937 and BD+26°3578) are on the order of 0.02 dex and are smaller than the other errors (see below), those for the other fainter stars are 0.06 – 0.18 dex, depending on the S/N of the spectra.

The equivalent widths of the Li doublet are determined by integrating the flux density of the synthetic spectra calculated for the final Li abundance as mentioned in § 2. The values are listed in Table 4.

3.4. Uncertainties

In addition to the above fitting errors, the uncertainties in the adopted continuum levels, macro-turbulence, and atmospheric parameters should be considered. The continuum level is estimated for the wavelength range around the Li doublet, in which 25 (in the case of two pixel binning) or 50 (in the case of no binning) data points exist. The uncertainty is 0.1% or smaller for the four bright stars ($S/N \gtrsim 300$), while it is approximately 0.5% for the spectra with $S/N \sim 50$. The effects of continuum level shifts of 0.1% and 0.5% are estimated to be 0.01 dex and 0.04 dex, respectively, by means of an analysis of the spectrum of G 64–12, in which the continuum level was changed artificially. The errors due to the uncertainty of the macro-turbulent velocity are on the order of 0.01 dex, as mentioned above.

The errors due to the uncertainties in atmospheric parameters are estimated by changing the parameters by $\delta(T_{\text{eff}}) = +100$ K, $\delta(\log g) = -0.3$ dex, and $\delta(v_{\text{micro}}) = +0.3$ km s⁻¹ for G 64–12. The effect of metallicity changes of 0.2 dex on the abundance analyses is negligible for extremely metal-poor stars. We confirmed that the effects of changes of $\log g$ and v_{micro} on the derived Li abundance are negligible. The Li abundance changes by +0.07 dex when the effective temperature is changed by +100 K. Such error estimates are scaled for the uncertainty for T_{eff} for each object listed in Table 2.

The total abundance errors ($\sigma[A(\text{Li})]_{\text{tot}}$) are obtained by adding, in quadrature, the fitting errors and the errors due to the uncertainty of the continuum placement, the macro-turbulence, and the effective temperature for each star (see Table 4).

3.5. Comparisons with Previous Work

Table 5 compares the results of the present study for stars in common with other recent studies. The T_{eff} and $A(\text{Li})$ of CS 22948–093 determined by this work and by Bonifacio et al. (2007) agree fairly well, while a significant discrepancy of $A(\text{Li})$ is found for CS 22965–054. This is clearly caused by the different effective temperatures adopted in the two analyses.

The abundances of BD+26°3578 were determined by Asplund et al. (2006) (where the star is referred to as HD 338529), adopting very similar atmospheric parameters ($T_{\text{eff}}, \log g$) = (6335 K, 4.04) to those of the present work (6340 K, 3.9). Their Fe abundance ($[\text{Fe}/\text{H}] = -2.26$ and $\log \epsilon(\text{Fe}) = 5.24$) from Fe II lines as well as the Li abundance agrees well with our result.

The T_{eff} 's of G 64–12 and G 64–37 determined by Boesgaard et al. (2005) are about 200 K lower than ours, which result in their lower $A(\text{Li})$ values. This is, however, partially compensated by the difference of model atmospheres used in the analysis. Boesgaard et al. adopted the grid of Kurucz (1993), which assumes convective overshooting. We found that the resulting $A(\text{Li})$ from this grid is systematically higher by 0.06 dex than that obtained from the no overshooting models by conducting analysis with both models. The discrepancy of $A(\text{Li})$ derived by us and Boesgaard et al. (2005) is explained by the differences of T_{eff} and the model atmosphere grid. The T_{eff} of Boesgaard et al. (2005) is spectroscopically determined by the analysis of Fe I lines. A systematic difference between T_{eff} 's from the excitation equilibrium and those from other methods (such as photometric colors) have been reported by previous studies (e.g., Norris et al. 2001; Barklem et al. 2005), which might be attributed to non-LTE effects on Fe line formation, although the recent work by Hosford et al. (2008) reported no discrepancy between the T_{eff} from LTE analyses of Fe I lines and T_{eff} from the H α profile analysis.

The T_{eff} 's determined by Ryan et al. (1999) are systematically lower than ours. The differences in T_{eff} for G 64–12, G 64–37 and CD –24°17504 are smaller than 100 K, while the differences are as large as 200 K for HD 84937 and BD+26°3578. The discrepancy of $A(\text{Li})$'s between the two studies are basically explained by the differences in the adopted effective temperatures.

The above comparisons demonstrate that the differences of derived Li abundances are due to differences of the effective temperature and/or the model atmosphere grid adopted in the analysis. These effects are systematic, and do not essentially affect the discussion of the slope or scatter of Li abundances if the same technique of effective temperature estimates and similar model atmosphere grids are used.

4. Discussion

4.1. Low Li Abundances for Extremely Metal-Poor stars

Figure 3 shows the Li abundances as a function of $[\text{Fe}/\text{H}]$ for our sample and others.⁴ We confirm that the Li abundance of the “reference” star BD+26°3578 ($[\text{Fe}/\text{H}] \sim -2.3$) determined by our analysis agrees well with the measurement by Asplund et al. (2006). By contrast, stars with $[\text{Fe}/\text{H}] < -3$ (the Extremely Metal-Poor, or EMP, stars) appear to have lower Li abundances on average, and also exhibit some scatter. We discuss this point further below.

The average of $A(\text{Li})$ (i.e., $\langle A(\text{Li}) \rangle$) of the eight stars with $[\text{Fe}/\text{H}] < -3$ is 2.03, with a sample standard deviation (σ) of 0.09 dex. The standard deviation is comparable with, or slightly smaller than, the measurement errors of our analysis (0.07–0.23 dex). Hence, we do not detect any significant scatter of the Li abundances in our sample of EMP stars. The $\langle A(\text{Li}) \rangle$ is lower by 0.24 dex and 0.20 dex than the the average of our two reference stars (2.27) and the average of the results of the LTE analysis by Asplund et al. (2006) for six stars in $-2.5 < [\text{Fe}/\text{H}] < -2.0$ (2.23), respectively. The difference of 0.2 dex is significant, compared to the $\sigma N^{-1/2} = 0.09/\sqrt{8} = 0.03$ dex, where N is the number of objects in the extremely metal-poor sample. We note that the Li abundances for stars in $-2.5 < [\text{Fe}/\text{H}] < -2.0$ are well determined by Asplund et al. (2006), and the scatter is small ($\sigma = 0.04$ dex and $\sigma N^{-1/2} = 0.02$ dex). We conclude that the Li abundances for stars with $[\text{Fe}/\text{H}] < -3$ are 0.2 dex lower than those of stars with higher metallicity on average, while no significant scatter or trend with metallicity is detected in our EMP sample. A similar conclusion was reached by Bonifacio et al. (2007); our new measurements for stars in the lowest metallicity range supports their results.

Such a difference can obviously be produced by a decreasing trend (slope) of $A(\text{Li})$ as a function of metallicity. The possible slope of $A(\text{Li})$ was discussed by Bonifacio et al. (2007) in detail. However, no clear physical reason for the slope, which appears only at the lowest metallicity range, has

⁴In the figure, the $[\text{Fe}/\text{H}]$ values of Bonifacio et al. (2007) and Asplund et al. (2006) are adopted without any correction. The solar Fe abundance adopted by Bonifacio et al. (2007) is 7.51, while that of Asplund et al. (2006) is determined by their own analysis of the solar spectrum. Asplund et al. (2006) also reported Fe abundances from Fe II lines, which are systematically higher by 0.08 dex than those from Fe I lines according to the authors. Hence, a possible shift of $[\text{Fe}/\text{H}]$ values by at most 0.1 dex should be taken into consideration in the comparisons of the three works.

yet been identified. Another possibility is that scatter of $A(\text{Li})$ increases in the range $[\text{Fe}/\text{H}] < -3$, and, as a result, the average decreases. This case would be relatively easily explained by depletion of Li, although some reason for the metallicity dependence of the depletion is also required.

If the effective temperatures estimated from the $(V-K)_0$ colors using the scales of Ramírez & Meléndez (2005a) and González Hernández & Bonifacio (2009) are employed, the Li abundances of our stars would be systematically higher. The effective temperatures derived using the scale of González Hernández & Bonifacio (2009) are systematically higher by 220 K and 150 K than the values from the Balmer line analysis for EMP stars and for stars with $[\text{Fe}/\text{H}] \sim -2.3$, respectively, resulting in 0.15 dex and 0.10 dex higher Li abundances. Although the difference of Li abundances between the EMP stars and less metal-poor stars becomes slightly smaller than the result derived adopting the effective temperature from the Balmer line analysis, the difference is still significant. By contrast, if the effective temperatures estimated using the scales of Ramírez & Meléndez (2005a) are adopted, the values are 290 K and 150 K higher than those from the Balmer lines, resulting in 0.20 dex and 0.10 dex higher Li abundances. In this case, the difference of Li abundances between the stars with $[\text{Fe}/\text{H}] < -3$ and > -2.5 is only 0.1 dex, which is no longer significant compared to our measurement errors.

4.2. Correlations with Stellar Parameters, Elemental Abundances, and Kinematics

Although no statistically significant scatter of $A(\text{Li})$ is found for our full EMP sample, within our measurement errors, the existence of *some* star-to-star differences in $A(\text{Li})$ is suggested. For instance, even if the stars with the largest measurement errors are excluded from the evaluation, a similar scatter of $A(\text{Li})$ remains. A difference of 0.14 dex is found in $A(\text{Li})$ for the two bright stars G 64–12 and G 64–37, as found by Boesgaard et al. (2005) and Nissen et al. (2005). In this subsection, we investigate correlations between $A(\text{Li})$ and the adopted stellar parameters, in order to search for a hint for understanding the lower Li abundances among the EMP stars.

Figure 4 shows $A(\text{Li})$ as a function of T_{eff} . No clear correlation can be seen in this figure. It should be noted that the random error of the effective temperature propagates into the derived Li abundance, which is represented by the arrows shown in the diagram. An increasing trend of Li abundance with decreasing T_{eff} is potentially influenced by this error.

Our sample includes stars that have already evolved to the subgiant branch. Their effective temperatures during the main-sequence stage should be higher than the current values, and might be as high as the hottest stars among the main-sequence sample. The stars having $\log g < 4.0$ are over-plotted by large circles representing candidate subgiants in the figure. If these stars are excluded, we find that stars cooler than 6150 K exhibit higher and almost constant Li abundances, while the warmer stars show some scatter. However, this probably reflects a metallicity effect, as the cooler stars (excluding subgiants) are objects having $[\text{Fe}/\text{H}] > -2$ studied by Asplund et al. (2006), while the warmer stars have $[\text{Fe}/\text{H}] < -2$. That is, the sample of very metal-poor stars ($[\text{Fe}/\text{H}] < -2$) have $T_{\text{eff}} > 6150$ K, or are subgiants. This could be due to a bias in the sample

selection caused by the fact that distant stars must be observed to cover lower metallicity ranges, and intrinsically faint stars are not sampled. Other than this point, no clear correlation appears between the Li abundances and effective temperature, even if subgiants are removed from the plot, or if the highest temperature among the sample (~ 6500 K) is assigned for them as their T_{eff} during their main-sequence phase.

Figure 5 shows Li abundances as functions of $[\text{Na}/\text{Fe}]$, $[\text{Mg}/\text{Fe}]$, and $[\text{Sr}/\text{Fe}]$. An anti-correlation between the Li abundance and the $[\text{Na}/\text{Fe}]$ ratio was reported for the globular cluster NGC 6752 by Pasquini et al. (2005). Such a trend is, however, not seen in our sample (Fig. 5): the two low Li stars HE 1148–0037 and SDSS 0040+16 have comparatively high $[\text{Na}/\text{Fe}]$ ratios, while that of the other low Li star, CS 22948–093, is low. If the NLTE effects on the Na abundances are taken into consideration, the abundances of less metal-poor stars become lower by about 0.3 dex. However, this correction does not result in any correlation between the Li and Na abundances.

No significant scatter is found for $[\text{Mg}/\text{Fe}]$ in our sample. Also, no correlation is found between the abundances of Li and the Mg abundances. In contrast, a large scatter of measured Sr abundances exists, which could reflect the contribution of a neutron-capture process that is efficient in the very early Galaxy (Truran et al. 2002; Travaglio et al. 2004; Aoki et al. 2005), as well as the contribution of the main r-process to higher metallicity objects. No correlation is found between the Li and Sr abundances, indicating that the Li production or depletion is not likely to be related to neutron-capture nucleosynthesis processes.

We are also interested in exploring whether the kinematics of the stars with lower $A(\text{Li})$ exhibit any peculiarities that distinguish them from the rest of the stars. For this exercise, we combined our present sample with that of Bonifacio et al. (2007). Proper motions of SDSS stars are listed in the public DR6 database, while those of other stars are taken from the NOMAD database (Zacharias et al. 2004). Distances were estimated from the luminosity classifications given by either the present paper or in Bonifacio et al. (2007), applying the methods described by Beers et al. (2000). Stars with $\log g > 4.0$ were considered dwarfs, those with $3.5 \leq \log g \leq 4.0$ were considered main-sequence turnoff stars, and those with $\log g < 3.5$ were considered subgiants. The adopted surface gravities, metallicities, photometry, distances, radial velocities, and proper motions are listed in Table 6. These data were used to derive the full space motions and other orbital information, following the procedures described by Carollo et al. (2007); results are listed in Table 7.

Figure 6 shows the derived rotational velocity with respect to the Galactic center, V_ϕ , as a function of $[\text{Fe}/\text{H}]$. The stars with low values of $A(\text{Li})$ are labeled by filled circles. We note that three stars with “normal” $A(\text{Li})$ are on highly prograde orbits (an additional star, CS 31061–0032, with $V_\phi = 205 \text{ km s}^{-1}$, may be a member of the metal-weak thick disk). This is somewhat unexpected, given the essentially zero net rotation of the inner halo, and net retrograde rotation of the outer halo. We plan to study these stars in more detail in the near future.

Based on the derived space velocities and orbital parameters, an attempt was made to assign approximate population memberships for these stars, listed in the second column of Table 7. The

assignments take into account the values of the velocity ellipsoids derived for the inner and outer halo, and the thick disk (including the metal-weak thick disk; D. Carollo et al., in preparation), as well as the derived Z_{\max} (the maximum distance from the Galactic plane in the vertical direction) for each star. We did not attempt to assign a membership to the four highly prograde stars, because, as was mentioned above, they require further investigation (FI in the second column of Table 7). Note that in some cases it was not possible to uniquely distinguish a single population assignment, so multiple assignments are given.

Inspection of these assignments indicates no tendency for the stars with low $A(\text{Li})$ to be associated preferentially with either the inner- or outer-halo populations. This is similar to the conclusions drawn by Bonifacio et al. (2007) based on inspection of radial velocities alone. However, the sample size (especially of low $A(\text{Li})$ stars) and the existing errors on the Li abundance determinations preclude a final determination.

4.3. Summary and Concluding Remarks

Our measurements of the Li doublet for extremely metal-poor stars based on the effective temperatures from the Balmer lines showed that the Li abundances in the metallicity range $[\text{Fe}/\text{H}] < -3$ are lower, on average, than for stars with higher metallicity. The same conclusion is also reached by adopting the effective temperatures from $(V-K)_0$ using the scales of Alonso, Arribas, & Martínez-Roger (1996) and González Hernández & Bonifacio (2009), although the Li abundances are systematically higher if the latter is adopted. If the temperature scale of Ramírez & Meléndez (2005a) for $(V-K)_0$ is adopted, the dependence of the Li abundances on metallicity becomes marginal.

Although no scatter or trend of Li abundances is detected within the sample of extremely metal-poor stars, the metallicity dependence of the Li abundance could be a key to understanding the Li problems found for metal-poor stars. Observations to obtain better quality spectra for such extremely metal-poor stars, to improve measurements of the Li feature itself, as well as for improved determination of T_{eff} from the $\text{H}\alpha$ and $\text{H}\beta$ profiles, will provide a useful constraint on the possible scenarios proposed to explain the Li problems. Moreover, measurements of Li abundances for even lower metallicity stars ($[\text{Fe}/\text{H}] < -3.5$) are also vital. Measurements of Li abundances in this metallicity range have been reported so far only for one system, a double-lined spectroscopic binary (CS 22876–032: Norris et al. 2000; González Hernández et al. 2008). We plan additional investigations of this metallicity range by high-resolution spectroscopic studies of extremely metal-poor star candidates discovered by the Hamburg/ESO survey and SDSS/SEGUE in the near future.

The authors would like to thank the anonymous referee for useful comments for improving this paper. W. A. is supported by a Grant-in-Aid for Science Research from JSPS (grant 18104003). P. S. B is a Royal Swedish Academy of Sciences Research Fellow supported by a grant from the Knut and Alice Wallenberg Foundation. P. S. B also acknowledges support from the Swedish Research

Council. T. C. B. acknowledges support from the US National Science Foundation under grants AST 04-06784 and AST 07-07776, as well as from grants PHY 02-16783 and PHY 08-22648; Physics Frontier Center/Joint Institute for Nuclear Astrophysics (JINA). N.C. acknowledges support from the Knut and Alice Wallenberg Foundation.

REFERENCES

- Alonso, A., Arribas, S., & Martínez-Roger, C. 1996, *A&A*, 313, 873
- Andrievsky, S. M., Spite, M., Korotin, S. A., Spite, F., Bonifacio, P., Cayrel, R., Hill, V., & François, P. 2007, *A&A*, 464, 1081
- Aoki, W., et al. 2005, *ApJ*, 632, 611
- Aoki, W., et al. 2006, *ApJ*, 639, 897
- Aoki, W., et al. 2008, *ApJ*, 678, 1351
- Asplund, M. 2005, *ARA&A*, 43, 481
- Asplund, M., Gustafsson, B., Kiselman, D., & Eriksson, K. 1997, *A&A*, 318, 521
- Asplund, M., Grevesse, N., & Sauval, A. J. 2005, *ASP Conf. Ser.* 336: *Cosmic Abundances as Records of Stellar Evolution and Nucleosynthesis*, 336, 25
- Asplund, M., Lambert, D. L., Nissen, P. E., Primas, F., & Smith, V. V. 2006, *ApJ*, 644, 229
- Barklem, P.S. 2007, *A&A*, 466, 327
- Barklem, P.S., Piskunov, N., & O’Mara, B.J. 2000, *A&A*, 363, 1091
- Barklem, P. S., Stempels, H. C., Allende Prieto, C. et al 2002, *A&A*, 385, 951
- Barklem, P. S., et al. 2005, *A&A*, 439, 129
- Beers, T. C., et al. 2007, *ApJS*, 168, 128
- Beers, T. C., & Christlieb, N. 2005, *ARAA*, 43, 531
- Boesgaard, A. M., Stephens, A., & Deliyannis, C. P. 2005, *ApJ*, 633, 398
- Bonifacio, P., et al. 2007, *A&A*, 470, 153
- Carollo, D., et al. 2007, *Nature*, 450, 1020
- Castelli, F., & Kurucz, R. L. 2003, *Modelling of Stellar Atmospheres*, 210, 20P
- Castelli, F., Gratton, R. G., & Kurucz, R. L. 1997, *A&A*, 318, 841

- Coc, A., Vangioni-Flam, E., Descouvemont, P., Adahchour, A., & Angulo, C. 2004, *ApJ*, 600, 544
- Cyburt, R. H., Fields, B. D. and Olive, K. A. arXiv:0808.2818
- Frebel, A., et al. 2005, *Nature*, 434, 871
- Frebel, A., Collet, R., Eriksson, K., Christlieb, N., & Aoki, W. 2008, *ApJ*, 684, 588
- Fuhrmann, K., Axer, M., Gehren, T., 1993, *A&A*, 271, 451
- González Hernández, J. I., & Bonifacio, P. 2009, arXiv:0901.3034
- González Hernández, J. I., et al. 2008, *A&A*, 480, 233
- Hosford, A., Ryan, S.G., García Pérez, A.E., Norris, J.E., and Olive, K.A. 2008, *A&A*, in press
- Kim, Y.-C., Demarque, P., Yi, S. K., & Alexander, D. R. 2002, *ApJS*, 143, 499
- Korn, A. J., Grundahl, F., Richard, O., Barklem, P. S., Mashonkina, L., Collet, R., Piskunov, N., & Gustafsson, B. 2006, *Nature*, 442, 657
- Korn, A. J., Grundahl, F., Richard, O., Mashonkina, L., Barklem, P. S., Collet, R., Gustafsson, B., & Piskunov, N. 2007, *ApJ*, 671, 402
- Korn, A. J., Richard, O., Mashonkina, L., Bessell, M. S., Frebel, A., & Aoki, W. 2009, arXiv:0903.3885
- Kurucz, R. L. 1993, CD-ROM 13, ATLAS9 Stellar Atmospheres Programs and 2 km/s Grid (Cambridge: Smithsonian Astrophys. Obs.)
- Munari, U., & Zwitter, T. 1997, *A&A*, 318, 269
- Nissen, P. E., Akerman, C., Asplund, M., Fabbian, D., & Pettini, M. 2005, *From Lithium to Uranium: Elemental Tracers of Early Cosmic Evolution*, 228, 101
- Noguchi, K. et al. 2002, *PASJ*, 54, 855
- Norris, J. E., Ryan, S. G., & Beers, T. C. 2001, *ApJ*, 561, 1034
- Norris, J. E., Beers, T. C., & Ryan, S. G. 2000, *ApJ*, 540, 456
- Pasquini, L., Bonifacio, P., Molaro, P., Francois, P., Spite, F., Gratton, R. G., Carretta, E., & Wolff, B. 2005, *A&A*, 441, 549
- Piau, L., Beers, T.C., Balsara, D.S., Sivarani, T., Truran, J.W., & Ferguson, J.W. 2006, *ApJ*, 653, 300
- Ramírez, I., & Meléndez, J. 2005a, *ApJ*, 626, 446

- Ramírez, I., & Meléndez, J. 2005b, *ApJ*, 626, 465
- Ryan, S. G., Beers, T. C., Deliyannis, C. P., & Thorburn, J. A. 1996, *ApJ*, 458, 543
- Ryan, S. G., Gregory, S. G., Kolb, U., Beers, T. C., & Kajino, T. 2002, *ApJ*, 571, 501
- Ryan, S. G., Norris, J. E., & Beers, T. C. 1999, *ApJ*, 523, 654
- Schlegel, D., Finkbeiner, D., & Davis, M. 1998, *ApJ*, 500, 525
- Skrutskie, M. F., et al. 2006, *AJ*, 131, 1163
- Smith, V. V., Lambert, D. L., & Nissen, P. E. 1998, *ApJ*, 506, 405
- Spergel, D. N., et al. 2003, *ApJS*, 148, 175
- Spite, M., & Spite, F. 1982, *Nature*, 297, 483
- Takeda, Y., Zhao, G., Takada-Hidai, M., Chen, Y.-Q., Saito, Y.-J., & Zhang, H.-W. 2003, *Chinese Journal of Astronomy and Astrophysics*, 3, 316
- Stehlé, C., & Hutcheon, R., 1999, *A&AS* 140, 93
- Travaglio, C., Gallino, R., Arnone, E., Cowan, J., Jordan, F., & Sneden, C. 2004, *ApJ*, 601, 864
- Truran, J. W., Cowan, J. J., Pilachowski, C. A., & Sneden, C. 2002, *PASP*, 114, 1293
- Tsuji, T. 1978, *A&A*, 62, 29
- Zacharias, N., Monet, D. G., Levine, S. E., Urban, S. E., Gaume, R., & Wycoff, G. L. 2004, *BAAS* 205.4815

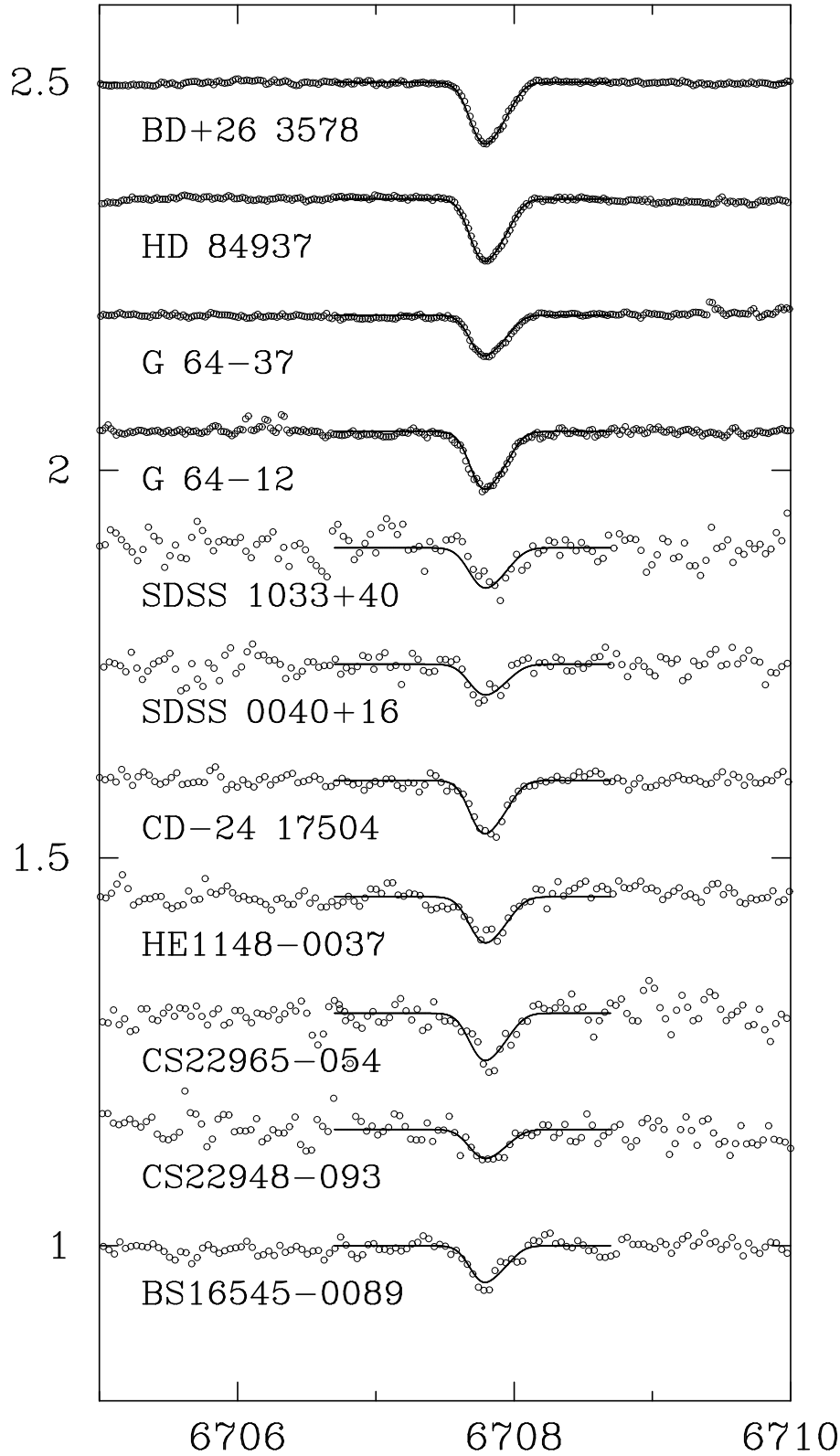


Fig. 1.— Spectra around the Li I resonance line. Open circles show the observed spectra normalized to the continuum level, which has been vertically shifted for presentation purposes. A synthetic spectrum for the derived Li abundance is over-plotted by a line for each star.

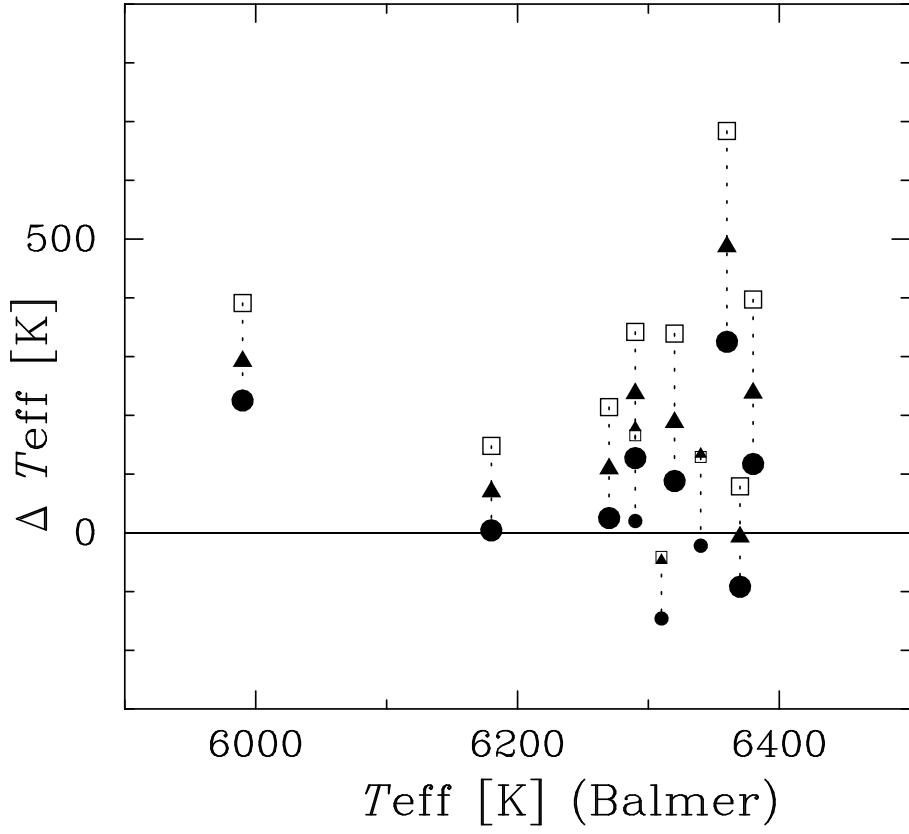


Fig. 2.— Comparisons of effective temperatures derived from the $(V - K)_0$ colors with those from the Balmer line analysis. The differences of the effective temperature from those from the Balmer line analysis are shown for the scales of Alonso, Arribas, & Martínez-Roger (1996) (circles), Ramírez & Meléndez (2005b) (squares), and González Hernández & Bonifacio (2009) (triangles).

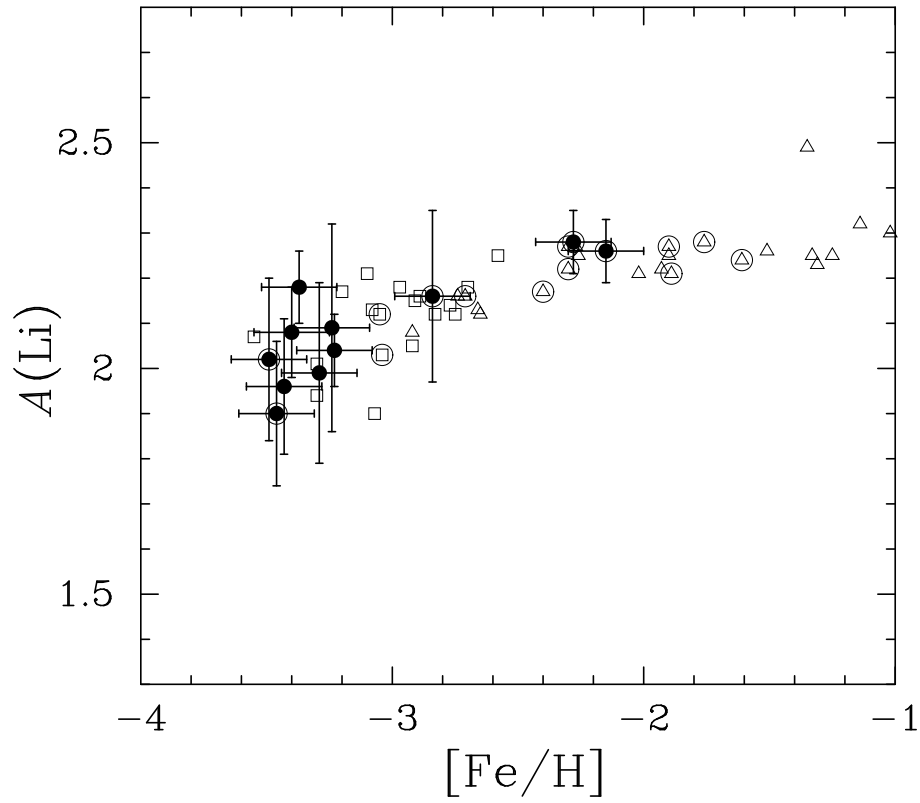


Fig. 3.— Li abundances as a function of $[\text{Fe}/\text{H}]$. The results of the present work are plotted by filled circles with error bars. The open triangles and squares indicate the results by Asplund et al. (2006) and Bonifacio et al. (2007), respectively. Large open circles are overplotted for subgiant stars ($\log g < 4.0$).

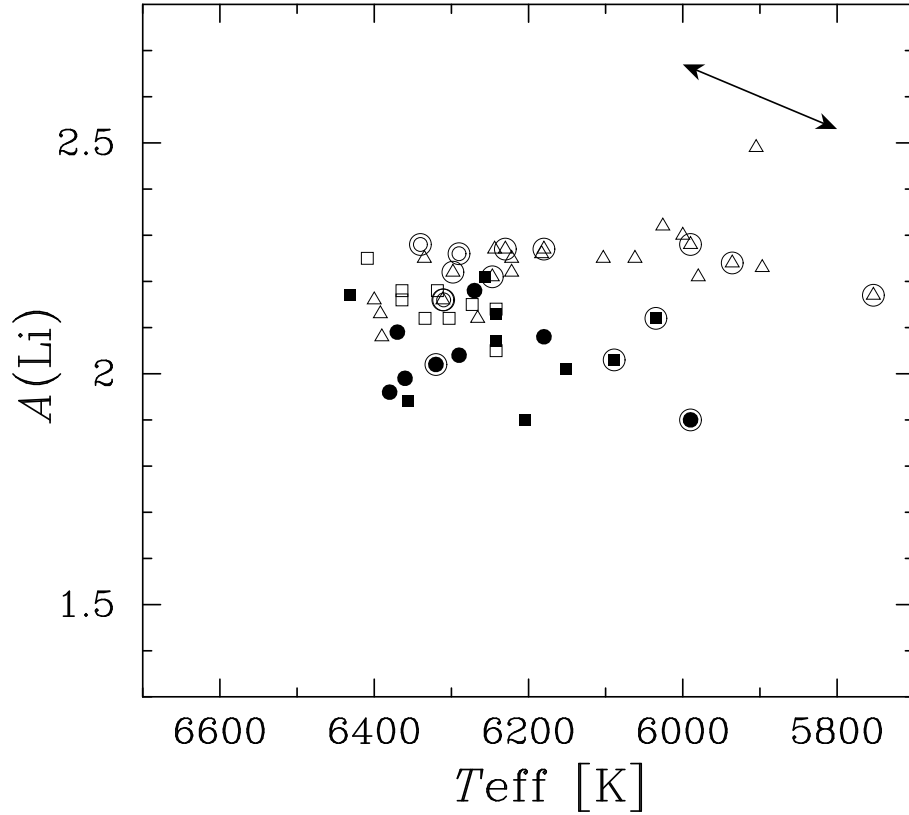


Fig. 4.— Li abundances as a function of effective temperature. The results of the present work are plotted by circles, while the triangles and squares indicate the results by Asplund et al. (2006) and Bonifacio et al. (2007), respectively. Filled symbols indicate stars having $[\text{Fe}/\text{H}] \leq -3.0$. Large open circles are overplotted for subgiant stars. The effect of $\delta T_{\text{eff}} = \pm 100 \text{ K}$ in the analysis on the Li abundance is shown by the arrow.

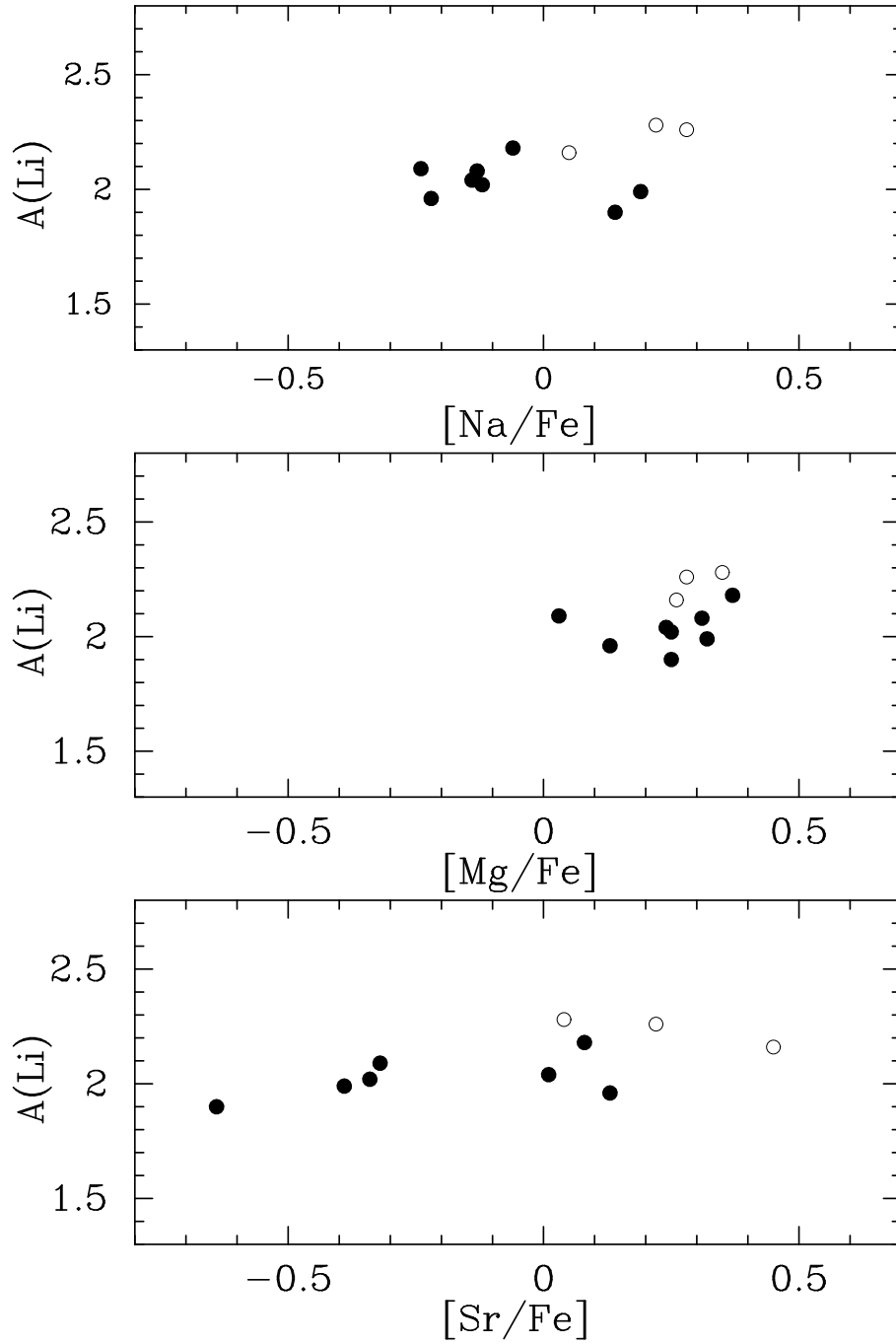


Fig. 5.— Li abundances as functions of $[\text{Na}/\text{Fe}]$, $[\text{Mg}/\text{Fe}]$, and $[\text{Sr}/\text{Fe}]$ for our sample. Filled circles indicate stars having $[\text{Fe}/\text{H}] \leq -3.0$. The upper limit of the Sr abundance of CD $-24^\circ 17504$ ($[\text{Sr}/\text{Fe}] < -0.9$) is not plotted in this figure.

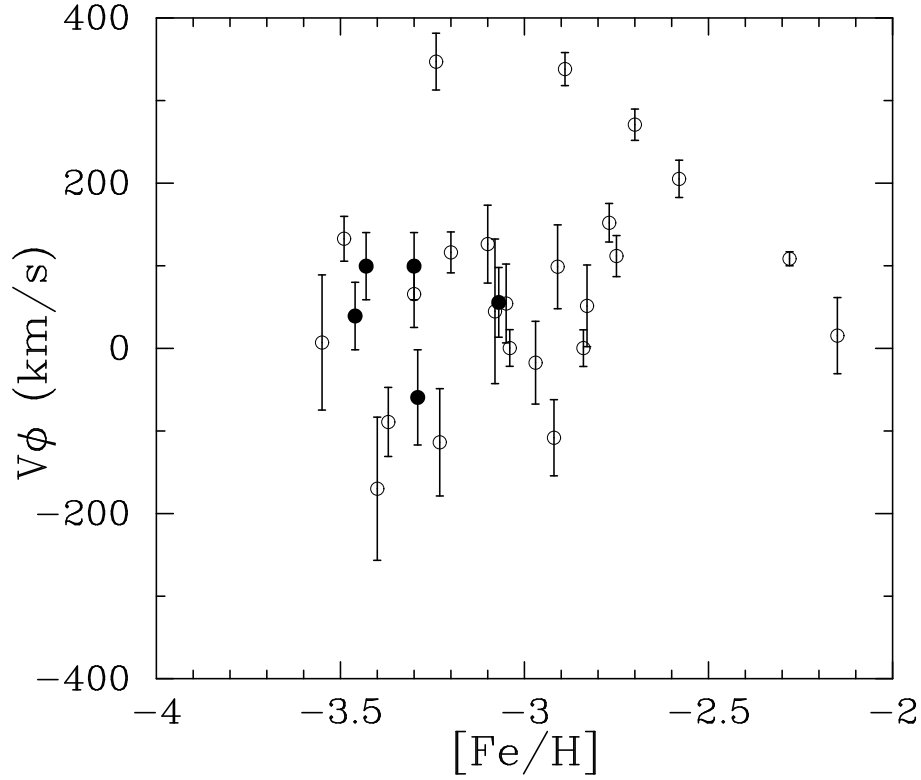


Fig. 6.— V_ϕ as a function of $[\text{Fe}/\text{H}]$ for our sample and that of Bonifacio et al. (2007). The filled circles indicate stars with $A(\text{Li}) < 2.0$, while the open ones indicate stars with $A(\text{Li}) > 2.0$. A typical error of Fe abundance determination is 0.15 dex. Note the presence of several stars with rather high V_ϕ .

Table 1. PROGRAM STARS AND OBSERVATIONS

Star	Obs. date	Exp. ^a	counts ^b	JD	V_H (km s ⁻¹) ^c
BS 16545–089	28 Feb. 2005	225	16,500	2453429.86	-161.54 ± 0.09
CS 22948–093	19 June 2005	174	5,900	2453541.06	369.24 ± 0.30
CS 22965–054	20 June 2005	100	5,000	2453541.97	-281.67 ± 0.20
HE 1148–0037	27 Feb. 2005	160	15,000	2453428.94	-10.88 ± 0.16
CD $-24^\circ 17504$	20 June 2005	20	14,000	2453542.12	136.61 ± 0.13
SDSS 0040+16 ^d	14 Sep. 2006	80	4,800	2453992.90	-49.43 ± 0.07
SDSS 1033+40 ^e	10 Feb. 2007	160	4,100	2454141.98	-132.87 ± 0.27
G 64–12	22 Feb. 2003	300	103,000	2453507.76	434.68 ± 0.03
G 64–37	18 May 2005	420	211,000	2453508.83	76.65 ± 0.06
HD 84937	22 Feb. 2003	180	626,000	2452692.83	-14.63 ± 0.03
BD+26°3578 ^f	17 May 2005	132	342,000	2453508.00	-91.23 ± 0.03

^aExposure time (minutes)

^bPhoton counts per pixel at 6700 Å

^cHeliocentric radial velocity

^dSDSS J004029.17+160416.2 = 0418-51884-574

^eSDSS J103301.41+400103.6 = 1430-53002-498

^f= HD 338529

Table 2. ATMOSPHERIC PARAMETERS

Object	$T_{\text{eff}}(\text{H}\alpha)$ (K)	$T_{\text{eff}}(\text{H}\beta)$ (K)	$T_{\text{eff}}(\text{adopted})$ (K)	$\sigma(T_{\text{eff}})$ (K)	$\log g$	v_{micro} (km s ⁻¹)	$A(\text{Fe})_{\text{FeI}}$	$A(\text{Fe})_{\text{FeII}}$
BS 16545–089	6380	6290	6320	150	3.9	1.5	3.96	3.88
CS 22948–093	6320	6410	6380	150	4.4	1.5 ^a	4.02	4.02
CS 22965–054	6390	6270	6310	200	3.9	1.5 ^a	4.61	4.56
HE 1148–0037	6100	5940	5990	200	3.7	1.5	3.99	3.90
CD $-24^\circ 17504$	6150	6190	6180	150	4.4	1.5	4.05	4.17
SDSS 0040+16	6350	6360	6360	200	4.4	1.5 ^a	4.16	4.25
SDSS 1033+40	6380	6370	6370	200	4.4	1.5 ^a	4.22	4.29
G 64–12	6260	6280	6270	100	4.4	1.5	4.08	4.20
G 64–37	6310	6280	6290	100	4.4	1.5	4.23	4.33
HD 84937	6330	6270	6290	100	3.9	1.2	5.30	5.35
BD+26°3578	6370	6330	6340	100	3.9	1.5	5.17	5.20

^aAssumed values (see text).

Table 3. PHOTOMETRY DATA AND EFFECTIVE TEMPERATURE

Star	V	$B - V$	$V - K$	$E(B - V)_{\text{SFD}}^{\text{a}}$	$E(B - V)_{\text{Na}}^{\text{a}}$	$E(B - V)_{\text{adopt}}^{\text{a}}$	$T_{\text{eff}}(V - K)^{\text{b}}$ [K]		
							A96	RM05	GH09
BS 16545–089	14.450	0.318	1.248	0.026	0.020	0.023	6408	6659	6508
CS 22948–093	15.180	0.360	1.175	0.018	0.008	0.013	6497	6777	6618
CS 22965–054	15.069	0.497	1.620	0.089	0.131	0.110	6180	6269	6263
HE 1148–0037	13.614	0.404	1.342	0.022	...	0.022	6215	6381	6282
CD $-24^{\circ}17504$	12.18	0.33	1.373	0.025	0.027	0.027	6184	6328	6250
SDSS 0040+16	15.231	0.310	1.202	0.047	0.058	0.052	6685	7044	6847
SDSS 1033+40	15.990	0.360	1.289	0.013	0.018	0.015	6278	6449	6363
G 64–12	11.453	0.385	1.245	0.028	0.003	0.003	6295	6484	6379
G 64–37	11.140	0.370	1.217	0.027	0.014	0.014	6417	6632	6527
HD 84937	8.28	0.41	1.218	0.037	0.007	0.007	6310	6456	6469
BD+ $26^{\circ}3578$	9.37	0.35	1.226	1.106	0.010	0.010	6318	6469	6474

^a $E(B - V)$ estimated from the dust maps of Schlegel et al. (1998) [$E(B - V)_{\text{SFD}}$], and from the interstellar Na I D line [$E(B - V)_{\text{Na}}$], as well as the adopted value [$E(B - V)_{\text{adopt}}$].

^bEffective temperatures estimated from $(V - K)_0$ using the scale of A96 (Alonso, Arribas, & Martínez-Roger 1996), RM05 (Ramírez & Meléndez 2005b), and GH09 (González Hernández & Bonifacio 2009).

Table 4. Li AND OTHER ELEMENTAL ABUNDANCES

Object	[Fe/H]	W (mÅ)	$A(\text{Li})$	$\sigma[A(\text{Li})]_{\text{fit}}$	$\sigma[A(\text{Li})]_{\text{tot}}$	[Na/Fe]	[Mg/Fe]	[Sr/Fe]
BS 16545–089	–3.49	15.3	2.02	0.12	0.17	–0.12	0.25	–0.34
CS 22948–093	–3.43	12.4	1.96	0.12	0.17	–0.22	0.13	0.13
CS 22965–054	–2.84	20.3	2.16	0.12	0.19	0.05	0.26	0.45
HE 1148–0037	–3.46	19.3	1.90	0.08	0.17	0.14	0.25	–0.64
CD $-24^{\circ}17504$	–3.40	21.2	2.08	0.06	0.13	–0.13	0.31	< –0.9
SDSS 0040+16	–3.29	13.6	1.99	0.14	0.20	0.19	0.32	–0.39
SDSS 1033+40	–3.24	16.5	2.09	0.18	0.23	–0.24	0.03	–0.32
G 64–12	–3.37	22.4	2.18	0.02	0.07	–0.06	0.37	0.08
G 64–37	–3.23	16.2	2.04	0.02	0.07	–0.14	0.24	0.01
HD 84937	–2.15	24.7	2.26	0.02	0.07	0.28	0.28	0.22
BD+ $26^{\circ}3578$	–2.28	23.7	2.28	0.02	0.07	0.22	0.35	0.04

Table 5. COMPARISON WITH PREVIOUS WORK

Object	this work		previous work (1)			previous work (2)		
	$T_{\text{eff}}(\text{K})$	$A(\text{Li})$	$T_{\text{eff}}(\text{K})$	$A(\text{Li})$	ref.	$T_{\text{eff}}(\text{K})$	$A(\text{Li})$	ref.
CS 22948–093	6380	1.96	6356	1.94	Bonifacio et al. (2007)			
CS 22965–054	6310	2.16	6089	2.03	Bonifacio et al. (2007)			
BD+26°3578	6340	2.28	6335	2.25	Asplund et al. (2006)	6150	2.15	Ryan et al. (1999)
G 64–12	6270	2.18	6074	2.15	Boesgaard et al. (2005)	6222	2.14	Ryan et al. (1999)
G 64–37	6290	2.04	6122	1.97	Boesgaard et al. (2005)	6240	2.09	Ryan et al. (1999)
CD –24°17504	6180	2.08				6070	1.97	Ryan et al. (1999)
HD 84937	6290	2.26				6160	2.17	Ryan et al. (1999)

Table 6. Surface Gravities, Metallicities, Photometry, Distance Estimates, Radial Velocities, and Proper Motions

Star Name	$\log g$	[Fe/H]	V	$B - V$	$E(B - V)$	Dist (kpc)	V_r (km s ⁻¹)	μ_α	σ_{μ_α}	μ_δ	σ_{μ_δ}
								(mas yr ⁻¹)			
BS 16023-0046	4.50	-2.97	14.170	0.378	0.017	0.935	-7.5	-40.0	2.0	-40.0	1.0
BS 16968-0061	3.75	-3.05	13.260	0.430	0.048	0.712	-80.7	-38.0	11.0	-36.0	8.0
BS 17570-0063	4.75	-2.92	14.510	0.330	0.039	1.275	-184.4	38.0	4.0	-30.0	1.0
CS 22177-0009	4.50	-3.10	14.270	0.401	0.044	0.869	-208.4	11.8	5.9	-62.5	5.8
CS 22888-0031	5.00	-3.30	14.900	0.413	0.014	0.968	-125.1	47.1	5.2	-20.6	5.2
CS 22948-0093	4.25	-3.30	15.180	0.360	0.015	1.346	364.3	-15.6	5.1	-22.8	4.8
CS 22953-0037	4.25	-2.89	13.640	0.367	0.027	0.753	-163.3	31.3	6.1	37.0	6.1
CS 22965-0054	3.75	-3.04	15.069	0.497	0.131	1.532	-281.5	26.0	1.0	0.0	3.0
CS 22966-0011	4.75	-3.07	14.555	0.422	0.013	0.830	-13.5	15.1	6.0	-42.2	6.0
CS 29499-0060	4.00	-2.70	13.030	0.370	0.019	0.726	-58.7	15.4	4.9	22.4	4.9
CS 29506-0007	4.00	-2.91	14.180	0.382	0.045	1.189	56.4	-3.6	7.9	-30.3	7.9
CS 29506-0090	4.25	-2.83	14.330	0.399	0.046	1.035	-21.3	-12.5	7.9	-39.1	7.9
CS 29518-0020	4.50	-2.77	14.003	0.415	0.023	0.741	-22.2	26.1	4.8	-10.4	4.8
CS 29518-0043	4.25	-3.20	14.566	0.371	0.019	1.064	144.8	26.0	5.0	-6.0	1.0
CS 29527-0015	4.00	-3.55	14.260	0.400	0.021	1.114	50.9	48.6	12.8	-22.5	12.8
CS 30301-0024	4.00	-2.75	12.950	0.420	0.064	0.646	-67.7	-33.8	1.8	-23.1	1.7
CS 30339-0069	4.00	-3.08	14.750	0.360	0.009	1.572	34.9	22.0	5.0	-16.0	12.0
CS 31061-0032	4.25	-2.58	13.874	0.409	0.036	0.818	21.0	-1.3	5.6	-11.6	5.7
BS 16545-0089	3.90	-3.49	14.450	0.318	0.023	1.356	-161.5	14.0	2.0	-22.0	3.0
CS 22948-0093	4.40	-3.43	15.180	0.360	0.013	1.346	369.2	-15.6	5.1	-22.8	4.8
CS 22965-0054	3.90	-2.84	15.069	0.497	0.110	1.532	-281.7	26.0	1.0	0.0	3.0
HE 1148-0037	3.70	-3.46	13.614	0.404	0.022	0.844	-10.9	-46.0	8.0	-42.0	1.0
CD -24°17504	4.40	-3.40	12.180	0.330	0.027	0.386	136.6	202.0	2.3	-185.8	1.6
SDSS 0040+16	4.40	-3.29	15.231	0.310	0.052	1.714	-49.4	24.0	4.0	-20.0	2.0
SDSS 1033+40	4.40	-3.24	15.990	0.360	0.015	2.150	-132.9	7.7	6.2	14.7	6.5
G 64-12	4.40	-3.37	11.453	0.385	0.003	0.217	434.7	-230.4	2.4	-80.3	1.8
G 64-37	4.40	-3.23	11.140	0.370	0.014	0.210	76.7	-54.3	3.6	-399.5	1.8
HD 84937	3.90	-2.15	8.280	0.410	0.007	0.073	-14.6	373.8	1.2	-774.7	0.4
BD+26°3578	3.90	-2.28	9.370	0.350	0.010	0.137	-91.2	0.9	0.6	-172.4	1.4

Table 7. $A(\text{Li})$ and Derived Kinematic Parameters

Star Name	Pop ^a	$A(\text{Li})$	U (km s ⁻¹)	V (km s ⁻¹)	W (km s ⁻¹)	V_ϕ (km s ⁻¹)	ecc	r_{max} (kpc)	r_{min} (kpc)	Z_{max} (kpc)
BS 16023–0046	IH	2.18	9	–237	30	–17	0.901	8.3	0.4	1.1
BS 16968–0061	IH	2.17	51	–165	–44	54	0.722	8.3	1.3	1.1
BS 17570–0063	IH/OH	2.05	60	–322	–45	–108	0.499	9.3	3.1	1.3
CS 22177–0009	IH/OH	2.20	–298	–80	147	126	0.840	32.8	2.8	13.9
CS 22888–0031	IH/OH	2.03	196	–153	50	65	0.788	12.5	1.4	2.8
CS 22948–0093	IH/OH	1.92	–329	–120	–201	99	0.854	38.3	3.0	30.9
CS 22953–0037	FI	2.16	191	109	89	338	0.677	37.2	7.1	8.0
CS 22965–0054	IH	2.06	250	–189	90	0	0.999	16.3	0.0	7.5
CS 22966–0011	IH	1.91	–19	–164	7	55	0.716	8.3	1.3	0.8
CS 29499–0060	FI	2.16	82	51	53	270	0.346	15.7	7.6	2.3
CS 29506–0007	IH	2.15	–106	–126	–56	98	0.557	8.8	2.5	1.8
CS 29506–0090	IH	2.10	–90	–172	24	51	0.758	8.6	1.1	0.8
CS 29518–0020	TD/IH	2.13	43	–68	38	152	0.304	8.8	4.7	1.2
CS 29518–0043	IH	2.14	85	–105	–121	116	0.453	10.3	3.8	4.6
CS 29527–0015	IH	2.08	150	–209	–81	7	0.970	11.3	0.1	2.9
CS 30301–0024	TD/IH	2.10	60	–108	–23	111	0.493	8.4	2.8	0.6
CS 30339–0069	IH	2.13	68	–176	–22	44	0.774	8.8	1.1	1.6
CS 31061–0032	TD	2.22	–19	–15	–33	205	0.073	9.1	7.9	0.9
BS 16545–0089	IH	2.02	–192	–87	–95	132	0.655	16.3	3.4	4.4
CS 22948–0093	OH	1.96	–332	–120	–205	99	0.857	39.8	3.0	32.4
CS 22965–0054	IH/OH	2.16	250	–190	90	0	1.000	16.3	0.0	7.5
HE 1148–0037	IH	1.90	71	–185	–124	39	0.727	9.29	1.47	5.8
CD –24°17504	OH	2.08	135	–388	–294	–169	0.607	28.9	7.0	23.7
SDSS 0040+16	IH/OH	1.99	91	–269	–110	–59	0.688	10.6	1.9	5.0
SDSS 1033+40	FI	2.09	–86	127	–101	347	0.602	37.1	9.2	9.8
G 64–12	OH	2.18	–48	–308	391	–89	0.657	40.2	8.3	39.0
G 64–37	IH/OH	2.04	–183	–332	–131	–113	0.642	14.3	3.1	6.1
HD 84937	IH	2.26	–214	–203	0	15	0.955	13.5	0.3	0.0
BD+26°3578	TD/IH	2.28	–51	–112	–52	108	0.497	8.7	2.9	0.9

^aAssigned Stellar Population – TD: Thick Disk (including Metal-Weak Thick Disk); IH: Inner Halo; OH: Outer Halo; FI: Further Inspection required